Published in final edited form as:
Exp Neurol. 2009 May ; 217(1): 124–135. doi:10.1016/j.expneurol.2009.01.022.

Cerebellar Pathology and Motor Deficits in the Palmitoyl Protein Thioesterase 1-Deficient Mouse

Shannon L. Macauley[1], **David F. Wozniak**[2], **Catherine Kielar**[4], **Yun Tan**[5], **Jonathan D. Cooper**[4], and **Mark S. Sands**[1,3,*]

1 *Department of Internal Medicine, Washington University School of Medicine, St. Louis, MO 63110*

2 *Department of Psychiatry, Washington University School of Medicine, St. Louis, MO 63110*

3 *Department of Genetics, Washington University School of Medicine, St. Louis, MO 63110*

4 *Pediatric Storage Disorders Laboratory, Department of Neuroscience and MRC Centre for Neurodegeneration Research, Institute of Psychiatry, King's College London, London SE5 9NU, UK*

5 *Department of Surgery, St Louis University School of Medicine, St Louis, MO 63104*

Abstract

Infantile neuronal ceroid lipofuscinosis (INCL, Infantile Batten Disease) is an inherited, neurodegenerative lysosomal storage disorder. INCL is the result of a *CLN1* gene mutation leading to a deficiency in palmitoyl protein thioesterase 1 (PPT1) activity. Studies in the forebrain demonstrate the PPT1-deficient mouse (PPT1−/−) mimics the clinical symptoms and underlying pathology of INCL; however, little is known about changes in cerebellar function or pathology. In this study, we demonstrate Purkinje cell loss beginning at 3 months, which correlates with changes in rotarod performance. Concurrently, we observed an early stage reactive gliosis and a primary pathology in astrocytes, including changes in S100β and GLAST expression. Conversely, there was a late stage granule cell loss, microglial activation, and demyelination. This study suggests that neuronal-glial interactions are the core pathology in the PPT1−/− cerebellum. In addition, these data identify potential endpoints for use in future efficacy studies for the treatment of INCL.

Introduction

Neuronal ceroid lipofuscinoses (NCLs), or Batten Disease, are a group of autosomal recessive, lysosomal storage diseases typified by central nervous system (CNS) involvement. As a class of disorders, the collective incidence of the NCLs is ~1:12,500 live births (Kohlschutter et al., 1993; Hofmann and Peltonen, 2001; Goebel and Wisniewski, 2004). Infantile neuronal ceroid lipofuscinosis (INCL) is one of the earliest onset and most rapidly progressing forms of NCL.

INCL is caused by mutations in the *CLN1* gene, leading to a deficiency in palmitoyl protein thioestersase 1 (PPT1) activity (Vesa et al., 1995; Hofmann et al., 2001; Mole et al., 2005). PPT1 is a lysosomal hydrolase ubiquitously expressed throughout the CNS and viscera. A deficiency in PPT1 activity leads to the accumulation of heterogenous material throughout the

*Corresponding Author: Mark S. Sands, Washington University School of Medicine, Department of Internal Medicine, Campus Box 8007, 660 S. Euclid Ave., St. Louis, MO 63110, Email: E-mail: msands@dom.wustl.edu, Phone: (314) 362-5494, Fax: (314) 362-9333.

neuroviscera, most notably in the brain. This storage material is autofluorescent and ultrastructurally identified as granular osmiophilic deposits (GRODS). The relationship between autofluorescent accumulation and disease pathology remains poorly understood (Haltia et al., 1973a; Haltia et al., 1973b).

Patients with INCL appear unaffected at birth and development proceeds normally until ~6–12 months. By 1 year, children show signs of mental retardation, microcephaly, motor dysfunction and visual deficits. In INCL, seizures appear between 16–24 months of age (Vanhanen et al., 1997). The average age of death is 6 years but some children survive into adolescence (Santavuori et al., 1973; Santavuori et al., 1974).

At autopsy, the CNS pathology of INCL is remarkable (Haltia et al., 1973). There is an overall brain atrophy, largely due to cortical thinning. Profound neuronal loss is present in the cerebral cortex, along with astrogliosis, microglial activation and macrophage infiltration. Neuronal cell loss is present in subcortical structures, largely in the thalamus. Purkinje and granule cell loss in the cerebellum is observed at autopsy. In addition to neurodegeneration and astrocyte activation, there is a loss of myelin at the end stage of disease.

A mouse model of PPT1-deficiency was created by a targeted disruption in the *CLN1* gene (Gupta et al., 2001). The initial characterization demonstrated that the PPT1-deficient mouse (PPT1−/−) shares many of the histological and clinical features of INCL (Bible et al., 2004; Griffey et al., 2004; Griffey et al., 2005; Kielar et al., 2007). Although mice develop normally, premature death occurs by 8.5 months. The brains accumulate autofluorescent storage material throughout the neuraxis (Bible et al., 2004). Phenotypically, these mice suffer from blindness (Griffey et al., 2005), seizures (Griffey et al., 2006; Kielar et al., 2007), cognitive deficits, and motor dysfunction (Griffey et al., 2004; Griffey et al., 2006). The cellular pathology of the CNS is profound with neuronal loss, brain atrophy, cortical thinning, gliosis and microglial activation.

Recently, Keilar and colleagues (2007) investigated the temporal changes in the forebrains of PPT1−/− mice. Although the work elegantly detailed the neuronal and glial pathology in the forebrain, little is known about the progression of the pathology and functional deficits in the cerebellum. Motor deficits are well documented in patients with INCL and cerebellar degeneration is present at autopsy. Initial observations in the PPT1−/− mice describe gait abnormalities and Purkinje cell loss (Gupta et al., 2001), but no further work has quantified these deficits or characterized the cellular mechanisms underlying these changes. In this study, we determined the temporal changes in cellular pathology in both neurons and glia. Concurrently, we quantified the progression of motor dysfunction. Taken together, these studies provide insight into the disease pathogenesis of INCL cerebellum and its relationship to motor function. Furthermore, it identifies potential end points to be used in future therapeutic studies for INCL.

Materials and methods

PPT1−/− Mice

PPT1−/− mice were created as previously described on a mixed background (Gupta et al., 2001). Subsequently, the mice were bred to C57Bl/6 mice for 10 generations to produce a congenic strain (Griffey et al., 2004). Wildtype (+/+) or PPT1-deficient (−/−) mice were generated by either heterozygous (+/−) or homozygous (−/−; +/+) matings at Washington University School of Medicine by M.S.S. Mouse genotype was determined by a PCR-based assay. Both male and female PPT1−/− mice and normal littermates (+/+) were used in this study. Animals were housed under a 12:12 hour light:dark cycle and were provided food and

water *ad libitum*. All procedures were carried out under an approved IACUC protocol from Washington University School of Medicine.

Cerebellar Weights

Seven month PPT1−/− (n=6) and wildtype littermates (n=5) were sacrificed via CO_2 aphyxiation and the brains harvested by a researcher blinded to genotype and age. A sharp knife was inserted coronally into the transverse sinus to separate the cerebellum from the forebrain. Similarly, a coronal cut was made immediately posterior to the cerebellum, separating the cerebellum from the medulla and spinal cord. Care was taken to ensure that the cut was flush with the back of the cerebellum. Each cerebellum was weighed using an analytical balance and group differences in weights were analyzed using an independent groups *t* test.

Quantification of Purkinje cells

Congenic PPT1−/− mice (n=3–6 per time point) and wildtype littermates (n=3–4 per time point) at 1, 3, 5, 6, and 7 mo. of age were used in this study. Briefly, mice were sacrificed via CO_2 asphyxiation, brains removed and post-fixed for 48 hours in 4% paraformaldehyde in phosphate buffered saline (PBS). Cerebella were separated from the forebrain and bisected in the sagittal plane about 1 mm off midline. The larger piece was embedded sagittally in paraffin and sectioned at 5μm through the midline. Sections were stained with hematoxylin & eosin (H&E). Counts of surviving Purkinje cells were made from midsagittal sections through the vermis for each lobe. Purkinje cells were counted if they possessed a well-defined cytoplasm and nucleus with the presence of a distinct nucleolus. Purkinje cells undergoing degeneration possessed a shrunken, pyknotic appearance with irregular margins and were not counted. The number of healthy Purkinje cells was recorded for each lobule (I through X) of the PPT1−/− and wild type cerebellum. For statistical analysis, data from wild type mice at the various ages counted (1–7 mos.) were collapsed and treated as a single wild type group. Previous work (Macauley et al., 2008) as well as data from this study demonstrated that Purkinje cell counts do not differ significantly over this age range. The Purkinje cell count data were analyzed by a repeated measures ANOVA model containing one between-subjects variable (groups) and one within-subjects variable (lobes), and subsequent pairwise comparisons. Bonferroni correction was used to maintain alpha levels at 0.05 when multiple comparisons were conducted.

Quantification of the Granular cell layer

To examine granule cell survival within lobule IV/V of the cerebellum, we used *StereoInvestigator* software (MicroBrightField Bioscience, Williston, VT) to obtain unbiased optical fractionator estimates of granule cell number from H&E stained sections. Cells were sampled using a series of counting frames distributed over a grid superimposed onto the section, with a random starting section chosen, followed by every fourth section thereafter. The sizes of the 'sampling grid' and of the 'dissector frame' used in this study were $250 \times 160\mu m^2$ and $20 \times 20\mu m^2$ respectively. Only clearly identifiable cells that fell within the dissector frame were counted, using a x100 oil objective.

The statistical significance of differences between genotypes of all quantitative data was assessed using a one-way ANOVA (SPSS 11.5 software, SPSS Inc, Chicago, IL), with statistical significance considered at $p \leq 0.05$. The mean coefficient of error (CE) for all individual optical fractionator and Cavalieri estimates was calculated according to the method of Gundersen and Jensen (1987) and was less than 0.08 in all analyses.

Immunohistochemistry for neuronal, astrocytic, & microglial markers

PPT1-deficient mice and wildtype littermates were sacrificed via CO_2 aphyxiation for immunohistochemistry at 1, 3, 5, 6 and 7 months of age. The brains were removed, fixed in 4% paraformaldehyde in phosphate buffer, and cryoprotected with 30% sucrose in tris-buffered saline (TBS). Brains were sectioned in the sagittal plane through the vermis (20μm) using a freezing cryostat. Adjacent, free floating sections were stained with the following antibodies: rabbit anti-glial fibrilllary associated protein (GFAP; 1:200 ImmunoStar, Inc.), rabbit anti-S100β (1:200; Abcam), rat anti-F4/80 (1:100; Serotec), mouse anti-calbindin (1:1000; Sigma), guinea pig anti-GLAST (1:2000; Chemicon) rabbit anti-GLT1 (1:100; Santa Cruz), and rabbit anti-glutamine synthetase (GS; 1:200 Santa Cruz). Briefly, sections were washed in tris-buffered saline (TBS), incubated in 1% H_2O_2 (Sigma) to quench endogenous peroxidase activity, and rinsed thoroughly in TBS. The tissue was blocked for 1 hour in 10% normal goat serum (NGS; Sigma), 0.25% Triton X-100 in TBS. Sections were incubated overnight at 4°C in primary antibodies in 5% NGS, 0.2% Triton X-100 in TBS. The following day the sections were rinsed in TBS and incubated in secondary antibodies (1:200; Vector Labs) in 10% NGS, 0.1% Triton X-100 in TBS for 75 minutes. The tissue was rinsed in TBS and then incubated in a peroxidase conjugated avidin-biotin complex (1:200; Vectastain Elite ABC kit from Vector Labs) for 1 hour at RT. Antibody immunoreactivity was visualized with 3′-3′ diaminobenzidine and H_2O_2 (DAB kit; Vector Labs) in TBS. Sections were dehydrated and coverslipped.

DeOlmos Cupric Silver Staining

Six, 7 and 8 mo. old PPT1−/− mice (n=2 per time point) and wildtype littermates (n=1–2 per time point) were deeply anesthetized with euthasol and transcardially perfused with 4% paraformaldehyde in sodium cacodylate buffer. The brains were removed and post-fixed for 48 hours. Each brain was embedded in a gelatin-based matrix (Switzer, 2000) and serial coronal sections (35 μm) were cut on a freezing microtome by Neuroscience Associates (Knoxville, TN). Neuronal degeneration was visualized by staining with a modified cupric silver method of DeOlmos (DeOlmos & Ingram, 1972; Switzer, 2000). A matrix of PPT1−/− and WT brains at identical levels in the coronal plane were stained simultaneously. Every sixth section (210 μm interval) was stained with the silver method and adjacent sections stained with H&E.

Luxol Fast Blue & PAS Stain

Seven-month-old PPT1−/− and wildtype littermates were sacrificed and sectioned at 20μm as described above. Every 12^{th} section throughout the vermis was stained with luxol fast blue and Periodic-acid Schiff stain.

TUNEL Staining

TUNEL staining was performed on sagittal sections throughout the cerebellum of PPT1−/− mice and wildtype littermates at 1, 3, 5, 6, and 7 months of age using the Apoptag Apoptosis Detection Kit (Milipore Corp) per the manufacturers instructions. Briefly, sections were warmed to room temperature (RT) and treated with proteinase K (20μg/ml) for 15 minutes at RT. Immediately following, endogenous peroxide was quenched with 1% hydrogen peroxide in methanol. After sections were incubated in equilibration buffer for 1 minute, working strength terminal deoxynucleotidyl transferase (TdT) enzyme was added to the tissue and incubated in a humidified chamber at 37°C. After a 60-minute incubation, the reaction was stopped by the addition of working strength stop/wash buffer for 10 minutes. An anti-digoxigenin conjugate was placed on each specimen for 30 minutes and the reaction visualized with DAB substate. The tissue was counterstained with nuclear fast red.

Rotarod Testing

Congenic PPT1−/− mice (n=11–14 mice per group) and wildtype littermates (n=11–14 mice per group) were tested on the constant speed rotarod (2.5 rpms) at 1, 3, 5, 6, and 7 months of age. Latency to fall served as the dependent variable and trials lasted a maximum of 60 s. At each age, mice received three test sessions where each session included a pretest trial on a stationary rod, followed by two test trials on the constant speed rotarod. To combat the effects of training, only the last test session was used in computing statistical differences with the previous two trials treated as training. A repeated measures ANOVA, including one between-subjects variable (genotype) and one within-subjects variable (age), was the main analysis conducted on monthly performance. Additional analyses (independent groups and paired *t* test, respectively) were performed on 1- and 7- month time points due to smaller sample sizes at these ages.

Results

Cerebellar Weights

Upon gross inspection at 7 mo. of age, the PPT1−/− cerebella appeared smaller than aged matched wildtype littermates (Figure 1A). The mean weight of PPT1−/− cerebella was 0.076g (SEM±0.0054) compared to 0.112g (SEM±0.0022) for normal littermates. At an end stage of disease (7 mo.), analysis of cerebellar weights (Figure 1B) demonstrated a significant loss of mass in the PPT1−/− mice, [$t(9) = 5.77$, $p < 0.0005$].

deOlmos Cupric Silver Staining

Silver staining was performed on 6, 7, and 8 mo. PPT1−/− mice and wildtype controls (Figure 2). Representative images of the anterior lobes of the cerebellum in the coronal plane are shown in Figure 2. As PPT1−/− mice aged, there was a progressive increase in neurodegeneration as visualized by silver staining (Figure 2B, C, D; respectively) when compared to normal (Figure 2A). When the CNS undergoes neurodegeneration, neurons bind silver causing individual cells and processes to appear ‘blackened’ with this staining method. Thus, at low magnification, diffuse silver staining was appreciable in the cerebellum at 6 mo. of age, most notably in the white matter tracts throughout the vermis and lateral hemispheres. As the mice aged, the intensity and distribution of staining increased to include ‘patches’ throughout the Purkinje cell and molecular cell layers. At 8 mo. of age, widespread neurodegeneration was evident in the anterior lobes of the cerebellum, although the staining was of equal or lower intensity.

Higher magnification images of a 7 mo. old PPT1−/− brain show parasagittal bands of degenerating Purkinje cells in the cerebellar cortex of the vermis and lateral hemispheres (Figure 2E, F). The molecular layer was littered with fragmented dendritic arbors associated with dying Purkinje cell neurons (Figure 2H). In addition to their dendritic arbors, the cerebellar white matter tracts, composed of afferant and efferent fibers, displayed an intense silver staining (Figure 2G, I).

Purkinje cell degeneration

The Purkinje cell layer in wild type mice consists of a one-cell-thick monolayer of contiguous Purkinje neurons nestled between the molecular and granular cell layers of the cerebellum (Figure 3B). In contrast, there was a clear disruption in the Purkinje cell layer in PPT1−/− mice (Figure 3B), immediately illustrating cell loss at 7 mo. of age throughout both the anterior-posterior as well as the medial-lateral axis of the cerebellum. Additionally, remaining Purkinje cells appeared unhealthy, presenting with a shrunken cytoplasm and a foamy appearance characteristic of lysosomal distension. To further investigate this apparent neuronal loss, Purkinje cell counts were performed throughout the vermis on each lobe (I-X) from wildtype

and PPT1−/− brains at 1, 3, 5, 6, and 7 mo. of age. At 5 mo. of age, there was a trend towards a decrease in total Purkinje cell number (13% decrease in total number; p=0.08). By 6 months of age, there was a statistically significant decrease in total Purkinje cell number (p=0.005) and culminated in a 50% reduction in total number at 7 mo. of age (p<0.0005; Figure 3C). Regionally, loss of Purkinje cells began at 3 mo. of age in the most anterior lobes. Although there was only a 3% decrease in total Purkinje cell number at 3 mo., there was a 23% decrease in cell number in lobe I/II compared to normal littermates (Figure 3D). By 5 mo., Purkinje cell death increased in posterior lobes. At 6 mo. of age, pairwise comparisons conducted for each lobe showed significant cell loss (beyond Bonferroni correction) in lobes I/II (p=0.039), IV/V (p=0.019), VI (p=0.001), VII (p=0.018), and VIII (p=0.003), with lobes IX and X spared. All lobes suffer a ≥50% reduction in Purkinje cell number by 7 mo. of age (p≤0.001). No change in Purkinje cell number is observed in PPT1−/− mice at 1 mo. of age.

In addition to quantifying neuronal loss, we investigated the morphology of the remaining neurons as an indicator of their general health. To examine any gross changes seen in Purkinje cell morphology, a time course of PPT1−/− and wildtype control brains were stained with an antibody against the calcium binding protein, calbindin. At low magnification, calbindin-stained Purkinje cells from lobe IV/V appeared indistinguishable in PPT1−/− brains compared to age-matched normal littermates at 1 mo. of age (Figure 3E). A contiguous layer of calbindin-positive cell bodies occupied the Purkinje cell layer, while the molecular layer was filled with a network of darkly stained dendritic arbors (black arrows). In addition, axonal projections from the Purkinje cell layer were observed transversing the granular cell layer. At 3 mo., gaps in calbindin-positive staining were appreciable at low magnification in the anterior lobes (I–V) of the PPT1−/− cerebellum, consistent with our counts of Purkinje cell number. At higher magnification, there was a decrease in the density of staining within the molecular layer demonstrating a pruning of dendritic arbors of the Purkinje cell neurons. By 5 mo. of age, numerous disruptions in calbindin staining throughout the anterior-posterior axis of the cerebellum were seen at low magnification. At higher magnification, the molecular layer appeared disorganized while the axonal projections through the granular cell layer looked fractured and swollen. By 7 mo. of age, Purkinje cell loss was widespread, with large gaps in staining throughout the cerebellar vermis. In addition, frank cell loss was appreciable in the lateral hemispheres of the cerebellum similar to the vermis (data not shown). On closer inspection, the soma of Purkinje neurons often displayed irregular margins with little to no dendritic arborization observed. Where arbors remained, swollen dendrites in Purkinje cells were observed (Figure 3E; white arrow). In addition to the profound Purkinje cell death that occurs in the PPT1−/− cerebellum, the remaining Purkinje cells, even at an early time point, appeared unhealthy.

Apoptosis and Assessment of Granular Cell Loss

Although widespread Purkinje cell loss occurs at a variety of ages, the only TUNEL-positive profiles were observed within the granular cell layer on PPT1−/− mice at 7 mo. of age (Figure 4A). To investigate granule cell loss, cell counts in the granular cell layer were performed throughout the vermis of lobe IV/V in wildtype and PPT1−/− brains at 1, 5 and 7 mo. (Figure 4). At 7 mo. of age, there was a statistically significant [$F(1,4) = 44.37$, $p = 0.003$] decrease in total number of cells within the granular cell layer in PPT1−/− mice. Total cell number was estimated to be 3.46×10^5 within lobe IV/V of mutant mice compared to 4.47×10^5 in age-matched wildtype controls (Figure 4B). This represents a 23% percent cell loss in the granular cell layer at 7 mo. of age. At earlier time points investigated, there was no decrease in the number of granule cells in lobe IV/V, suggesting this loss of neurons is a later stage phenomenon.

Astrocyte activation

Astrocyte activation, visualized by glial fibrillary associated protein (GFAP) upregulation, began at an early age (Figure 5A). At 1 mo. of age, there was a slight increase in GFAP staining in PPT1−/− mice compared to wildtype controls. By 3 mo., the Bergmann glia (Golgi epithelial cells) displayed a clear increase in GFAP immunoreactivity both at the cell body and within their processes. At low magnification, this staining appeared 'patchy' throughout the A-P axis of the cerebellum. Astrocyte activation continued to increase at 5 mo. of age, and by 7 mo., the entire molecular layer throughout the vermis of lobes I-X was strongly immunoreactive for GFAP. At high magnification, there was an increase in number of GFAP-stained Bergmann glial processes in the molecular layer as well as an apparent hypertrophy of individual glial processes.

Astrocyte Dysfunction

In an effort to quantify astrocyte cell number, S100β staining, a calcium binding protein largely localized to astrocytes, was performed on cerebella from PPT1−/− and wildtype littermates (Figure 5B). As the PPT1−/− mice aged, there was an overall decrease in S100β staining throughout the cerebellum. In the wild type control, S100β-positive cell bodies were mostly localized within the granular and Purkinje cell layers. Diffuse staining of Bergman glial fibers was also apparent within the molecular layer. By 3 mo. of age, the PPT1−/− cerebella showed a decrease in the intensity of S100β immunoreactive cell bodies, most notably within the granular cell layer. As the mice age, the S100β-positive Bergman glia, with their cell bodies intermixed with Purkinje neurons in the Purkinje cell layer, demonstrated a loss of immunoreactivity. In addition, there was a diffuse loss of S100β staining within all layers of the 7 mo. PPT1−/− cerebellum. S100β-positive cell bodies were absent from both the Purkinje cell and granular cell layers.

Glutamine Synthetase (GS), GLAST, & GLT-1 Immunohistochemistry

To further investigate whether the loss of S100β immunoreactivity was due to changes in protein expression or due to a loss of astrocytes, we used a second astrocyte marker, glutamine synthetase (GS), to stain 7 mo. old wildtype and PPT1−/− mice (Figure 6). There was a decrease in GS staining in the 7 mo. PPT−/− cerebellum compared to normal controls. Although there was an appreciable loss of neuropil in the PPT1−/− cerebellum at 7 mo., the remaining cells in the granular cell layer stained for GS. Qualitatively, the number of GS-positive cell bodies in the molecular layer seemed less than the wild type control. Importantly, there was a considerable decrease in the number of GS-immunoreactive cell bodies in the Purkinje cell layer, suggestive of a loss of Bergman glia at 7 mo. of age.

Given the number of changes observed in PPT1−/− astrocytes, we performed immunohistochemistry staining for several astrocyte specific glutamate transporters, GLAST and GLT-1, in PPT1−/− and wild type mice (Figure 6). At low magnification, the wild type-Bergman glia were largely immunoreactive for GLAST, with punctate staining present in the Purkinje cell and molecular layers. In contrast, the PPT1−/− cerebellum at 7 mo. of age suffered an overall decrease in GLAST immunoreactivity. At higher magnification, this change in protein expression was most notable in the Bergmann glial processes in the molecular layer, with a near complete loss of staining at 7 mo. of age.

Although GLAST expression was altered in the PPT1−/− mice, GLT-1 staining in the cerebellar folia seemed relatively unchanged when compared to wildtype littermates. The major change in GLT-1 staining in mutant mice coincided with a loss of Purkinje cells at 7 mo. of age. The normal pattern of GLT-1 staining circumscribes the Purkinje cell bodies and in their absence in mutant mice, this staining is lost. Otherwise, comparable patterns and levels

of GLT-1 staining were apparent in both PPT1−/− and wildtype cerebella in the granular cell and molecular layers.

Microglial Reactivity

PPT1−/− and wildtype brains were stained for F4/80, a marker for microglia and macrophages (Figure 7). Prior to 5 mo. of age, there was no detectable F4/80 staining within the brains PPT1 −/− mice or wildtype littermates. At 5 mo. of age, an increase in F4/80 staining was evident in the PPT1−/− cerebellum. The F4/80-positive cells, mostly comprised of small-ramified cells, were evenly dispersed throughout the molecular, Purkinje cell, and granular cell layers. As the mice age, there was a progressive increase in the number of positively stained cells in the PPT1 −/− cerebellum. In addition, the morphology of the positive cells changed from small ramified cells (A) to large, round cells with brain macrophage-like morphology (B) as the mice age.

Luxol Fast Blue and Periodic acid Schiff staining

Luxol Fast Blue (LFB) and Periodic acid Schiff (PAS) staining were performed on 7 mo. old PPT1−/− mice and normal littermates (Figure 8). Upon gross examination, the white matter tracts, as visualized by LFB, appeared thinner in PPT1−/− mice (arrows) compared to normal littermates. At higher magnification, LFB staining revealed an array of densely stained myelinated fibers traversing through the white matter in the wildtype mouse. In contrast, the PPT1−/− cerebellar white matter appeared disorganized, less intensely stained and littered with ‘holes’. Furthermore, the number of densely stained cell bodies in the white matter was decreased and the morphology of the remaining cell bodies appeared shrunken and irregular in PPT1−/− mice. These densely stained cells are glia, most likely oligodendrocytes, given their localization and organization in the cerebellar white matter.

PAS staining, a marker of glycogen storage was performed on 7 mo. PPT1−/− mice. There was a noticeable increase in the intensity of PAS staining in the vasculature of the white matter tracts (black arrows). In addition, PAS-positive cells were present in the molecular layer and Purkinje cell layers of the PPT1−/− cerebellum, but only at a late stage of disease (5–7 mo.).

Rotarod Testing

PPT1−/− mice and normal littermates were tested on the rotorod at 1, 3, 5, 6 and 7 mo. of age and latency to fall was recorded (Figure 9). At 1 mo. of age, the performance of PPT1−/− mice and normal littermates was indistinguishable on the rotorod (54.9s v. 54.7s; respectively). The latency to fall began to decrease in PPT1−/− mice compared to WT mice at 3 mo. of age (55.6s v. 48.9s; respectively), although this was not a significant change. By 5 mo. of age, the ability of the PPT1−/− mice to stay on the rotorad was significantly impaired (39.5s; $p \leq 0.0005$), while wildtype littermates continued to perform near criterion (55.9s). The performance of PPT1−/ − mice continued to decrease at 6 mo. (27.1s; $p<0.0005$) and reached a nadir at 7 mo. of age (1.8s; $p=0.001$). Repeated measures ANOVA revealed a significant main effect of group, [$F(1,26) = 68.75$, $p < 0.0005$], a significant effect of age, [$F(2,52) = 24.16$, $p < 0.0005$], and a significant group by age interaction, [$F(2,52) = 27.84$, $p < 0.0005$].

Discussion

Pathological changes within the PPT1−/− forebrain were described in detail (Kielar et al., 2007), however little is known about the morphological and functional changes localized to the hindbrain. Since reports of INCL patients describe profound cerebellar pathology and motor deficits, a complete characterization of the disease progression within the PPT1−/− cerebellum is essential. Our findings demonstrate that substantial pathology exists within the PPT1−/− cerebellum, consistent with the human course of disease. At an end stage of disease, there was significant cerebellar atrophy, suggesting profound cell loss in the PPT1−/− cerebella. We

performed silver degeneration staining to investigate which aspects of the cerebellum were most affected. Staining of the cerebellar white matter was first observed, suggesting the major afferent and efferent projections were undergoing widespread degeneration. Similarly, the molecular and Purkinje cell (PC) layers were argyrophillic, identifying 'patches' of degenerating PC bodies and dendritic arbors. As described by Sarna and Hawkes (2003), PCs in the cerebellum are highly organized into parasagittal bands (based on zebrin II immunoreactivity), which carry their own molecular fingerprint, and are differentially susceptible to toxic insults. Silver staining suggests that specific classes of PPT1−/− PCs are more susceptible to cell death than others.

Quantification of the PC layer showed a trend towards early neuronal loss. As described above, the death of PCs throughout each lobe was not random but rather a stereotyped wave of cell death beginning in the anterior lobes of the cerebellar vermis and later affecting the posterior lobes. Other LSDs such as Nieman Pick Type A/B (Sarna et al., 2001; Macauley et al., 2008), Nieman Pick Type C (Sarna and Hawkes, 2003), and late infantile neuronal ceroid lipofuscinosis (Sleat et al., 2004; Chang et al., 2008) detail a vulnerability of the PCs in the anterior lobes to cell death. Although the mechanism of differential Purkinje cell vulnerability in LSDs is unknown, some have postulated that increased levels of metabolic enzymes (Slemmer et al., 2007), increased glutamate transporter expression (EAAT4) (Welsh et al., 2002) and the presence of small heat shock proteins (Armstrong et al., 2000, 2001) is thought to be neuroprotective for PCs in the posterior lobes.

Although some PCs are initially more resistant to toxic insults in INCL, the posterior lobes still become affected later in disease progression. This phenomenon is consistent with other LSDs, but dissimilar to other cerebellar mutants (reviewed in (Sarna and Hawkes, 2003). Even if a subset of PCs survives longer than others, we hypothesize that their function is compromised based on the morphological changes observed (Figure 3).

Consistent with PC loss in the PPT1−/− cerebellum, there was an age-dependent decline in rotarod performance. Although not statistically significant, there was a trend for both PC loss and motor dysfunction at 3 months of age. Significant performance deficits ($p \leq 0.05$) on the constant speed rotarod are seen at 5 mos. of age, which coincides with a trend towards Purkinje cell loss that reaches significance at 6 mos. These data demonstrate a strong relationship between cerebellar pathology and function, a phenomenon seen in other LSDs (Macauley et al., 2008). Furthermore, there is a temporal correlation with the loss of neurons within motor pathways in the basal ganglia and thalamus (Kielar and Cooper unpublished observations), which may also contribute to this behavioral phenotype.

In contrast to PC loss, apoptotic cell death in the granular cell layer is a later stage phenomenon. These data illustrate a selective vulnerability of cerebellar neurons to cell death, an important consideration for therapeutic delivery and timing.

Although INCL is described as a neurodegenerative disorder, there is prominent astrocyte pathology in the PPT1−/− cerebellum. This pathology manifests itself as astrocyte activation, or gliosis, as well as a primary astrocyte deficit. Gliosis is often the first pathological change observed in the NCLs (Bible et al., 2004; Pontikis et al., 2005; Kielar et al., 2007; Chang et al., 2008), including the first pathological change seen in the PPT1−/− forebrain (Kielar et al., 2007). Similarly, activation of the PPT1−/− Bergmann glia was the first cerebellar change observed and this process intensified with age. In addition to an early stage gliosis, astrocytes are intrinsically dysfunctional. As previously reported, normal astrocytes express PPT1 (Margraf et al., 1999; Haltia, 2003), and PPT1-deficient astrocytes accumulate GRODs (Galvin et al., 2007). Our studies demonstrate a decrease in S100β staining at early stages in PPT1−/− mice, most notably in the Bergman glia. Interestingly, S100β staining is typically upregulated,

not down regulated in CNS injury (i.e. neurodegenerative disorders, traumatic brain injury, etc.), (Griffin et al., 1995; Mrak and Griffinbc, 2001; Rothermundt et al., 2003; Wainwright et al., 2004; Goncalves et al., 2008). This reduction of S100β in astrocytes could be due to the secretion of S100β into the extracellular space, a neurotoxic event in the adult brain (reviewed in (Donato, 2003), or due to astrocytic cell loss. We demonstrated a concurrent decrease in glutamine synthetase (GS) staining in the Bergman glia, suggesting at minimum, an astrocyte dysfunction or more likely, a loss of Bergman glia.

An overall decrease in GLAST expression, an astrocyte specific glutamate transporter, was observed in the aged PPT1−/− cerebellum. Furthermore, specific loss of GLAST was observed in the Bergman glia circumscribing PCs as well as in their glial processes in the molecular layer. Although comparable levels of GLT-1 were observed in the PPT1−/− cerebellum, GLAST is the main glutamate transporter in Bergman glia, thus demonstrating a potential disruption in glutamate recycling in the PPT1−/− cerebellum. Furthermore, localized changes in the expression of glutamate and both astrocytic and neuronal glutamate transporters are also evident in the thalamus, basal ganglia and hippocampus (Kielar and Cooper, unpublished observations), suggesting that altered glutamate/glutamine cycling may be an important feature of INCL pathogenesis.

Although changes in astrocytes and neurons occur at an early stage in INCL, changes in microglia and oligodendrocytes occur later. As the mice age, there is an increase in F4/80+ cells in the CNS as well as changes in their morphology (Figure 7A, B). We hypothesize that microglial activation is initially mounted in the PPT1−/− cerebellum to clear cellular debris, yet a secondary macrophage infiltration is present at the end stage of INCL.

Demyelination is seen in the aged PPT1−/− cerebellum. At autopsy, patients with INCL suffer a near complete loss of myelin in the CNS (Haltia, 2003). Not surprisingly, we found atrophy of the cerebellar white matter tracts as well as a loss of myelin components, such as CNPase (data not shown), in the PPT1−/− cerebellum. Whether this demyelination is due to the axonal death of PCs or a primary oligodendrocyte dysfunction requires further investigation.

This study provides a comprehensive characterization of cerebellar pathology and its relationship to motor dysfunction in INCL. We demonstrate cerebellar pathology is not restricted to neurons, and that a concurrent glial involvement, most notably in astrocytes, exists. We believe that perturbed neuron-glial interactions are the cause of CNS pathology in INCL. In addition, this study outlines a temporal and spatial description of cerebellar pathology, providing valuable endpoints for use in future therapy studies. Importantly, since clinical trials for LINCL and INCL are ongoing (Zhang et al., 2001; Taupin, 2006; Worgall et al., 2008), it identifies the need to target therapies not only to the forebrain of patients suffering from INCL, but also to the hindbrain. It also provides evidence of profound glial involvement and thus necessitates the development of therapies aimed at treating both neuronal and glial dysfunctions.

Acknowledgements

We would like to thank Neuroscience Associates (Knoxville, TN) for their consistent quality of silver degeneration staining. This work was supported by NIH grants (NS043105; MSS and NS41930; JDC), Ruth L. Kirschstein NRSA Fellowship (NS056728; SLM), grant support and a graduate studentship from the Batten Disease Support and Research Association (CK), and an NIH Neuroscience Blueprint Core Grant (P30 NS057105; DFW) to Washington University.

References

Armstrong CL, Krueger-Naug AM, Currie RW, Hawkes R. Constitutive expression of the 25-kDa heat shock protein Hsp25 reveals novel parasagittal bands of purkinje cells in the adult mouse cerebellar cortex. J Comp Neurol 2000;416:383–397. [PubMed: 10602096]

Armstrong CL, Krueger-Naug AM, Currie RW, Hawkes R. Constitutive expression of heat shock protein HSP25 in the central nervous system of the developing and adult mouse. J Comp Neurol 2001;434:262–274. [PubMed: 11331528]

Bible E, Gupta P, Hofmann SL, Cooper JD. Regional and cellular neuropathology in the palmitoyl protein thioesterase-1 null mutant mouse model of infantile neuronal ceroid lipofuscinosis. Neurobiol Dis 2004;16:346–359. [PubMed: 15193291]

Chang M, Cooper JD, Sleat DE, Cheng SH, Dodge JC, Passini MA, Lobel P, Davidson BL. Intraventricular enzyme replacement improves disease phenotypes in a mouse model of late infantile neuronal ceroid lipofuscinosis. Mol Ther 2008;16:649–656. [PubMed: 18362923]

Donato R. Intracellular and extracellular roles of S100 proteins. Microsc Res Tech 2003;60:540–551. [PubMed: 12645002]

Galvin N, Vogler C, Levy B, Kovacs A, Griffey M, Sands M. A murine model of infantile neuronal ceroid lipofuscinosis - Ultrastructural evaluation of storage in the central nervous system and viscera. Pediatr Dev Pathol 2007;1

Goebel HH, Wisniewski KE. Current state of clinical and morphological features in human NCL. Brain Pathol 2004;14:61–69. [PubMed: 14997938]

Goncalves CA, Leite MC, Nardin P. Biological and methodological features of the measurement of S100B, a putative marker of brain injury. Clin Biochem 2008;41:755–763. [PubMed: 18454941]

Griffey M, Macauley SL, Ogilvie JM, Sands MS. AAV2-mediated ocular gene therapy for infantile neuronal ceroid lipofuscinosis. Mol Ther 2005;12:413–421. [PubMed: 15979943]

Griffey M, Bible E, Vogler C, Levy B, Gupta P, Cooper J, Sands MS. Adeno-associated virus 2-mediated gene therapy decreases autofluorescent storage material and increases brain mass in a murine model of infantile neuronal ceroid lipofuscinosis. Neurobiol Dis 2004;16:360–369. [PubMed: 15193292]

Griffey MA, Wozniak D, Wong M, Bible E, Johnson K, Rothman SM, Wentz AE, Cooper JD, Sands MS. CNS-directed AAV2-mediated gene therapy ameliorates functional deficits in a murine model of infantile neuronal ceroid lipofuscinosis. Mol Ther 2006;13:538–547. [PubMed: 16364693]

Griffin WS, Yeralan O, Sheng JG, Boop FA, Mrak RE, Rovnaghi CR, Burnett BA, Feoktistova A, Van Eldik LJ. Overexpression of the neurotrophic cytokine S100 beta in human temporal lobe epilepsy. J Neurochem 1995;65:228–233. [PubMed: 7790864]

Gupta P, Soyombo AA, Atashband A, Wisniewski KE, Shelton JM, Richardson JA, Hammer RE, Hofmann SL. Disruption of PPT1 or PPT2 causes neuronal ceroid lipofuscinosis in knockout mice. Proc Natl Acad Sci U S A 2001;98:13566–13571. [PubMed: 11717424]

Haltia M. The neuronal ceroid-lipofuscinoses. J Neuropathol Exp Neurol 2003;62:1–13. [PubMed: 12528813]

Haltia M, Rapola J, Santavuori P. Infantile type of so-called neuronal ceroid-lipofuscinosis. Histological and electron microscopic studies. Acta Neuropathol 1973a;26:157–170. [PubMed: 4763201]

Haltia M, Rapola J, Santavuori P, Keranen A. Infantile type of so-called neuronal ceroid-lipofuscinosis. 2. Morphological and biochemical studies. J Neurol Sci 1973b;18:269–285. [PubMed: 4121459]

Hofmann, SL.; Peltonen, L. The neuronal ceroid lipofuscinosis. In: Scriver, CR.; Beaudet, AL.; Sly, WS.; Valle, D., editors. The Metabolic and Molecular Basis of Inherited Disease. New York: McGraw-Hill; 2001. p. 3877-3894.

Hofmann SL, Das AK, Lu JY, Soyombo AA. Positional candidate gene cloning of CLN1. Adv Genet 2001;45:69–92. [PubMed: 11332777]

Kielar C, Maddox L, Bible E, Pontikis CC, Macauley SL, Griffey MA, Wong M, Sands MS, Cooper JD. Successive neuron loss in the thalamus and cortex in a mouse model of infantile neuronal ceroid lipofuscinosis. Neurobiol Dis 2007;25:150–162. [PubMed: 17046272]

Kohlschutter A, Gardiner RM, Goebel HH. Human forms of neuronal ceroid-lipofuscinosis (Batten disease): consensus on diagnostic criteria, Hamburg 1992. J Inherit Metab Dis 1993;16:241–244. [PubMed: 8411970]

Macauley SL, Sidman RL, Schuchman EH, Taksir T, Stewart GR. Neuropathology of the Acid Sphingomyelinase Knockout Mouse Model of Niemann-Pick A Disease Including Structure-Function Studies Associated with Cerebellar Purkinje Cell Degeneration. Exp Neurol. 2008

Margraf LR, Boriack RL, Routheut AA, Cuppen I, Alhilali L, Bennett CJ, Bennett MJ. Tissue expression and subcellular localization of CLN3, the Batten disease protein. Mol Genet Metab 1999;66:283–289. [PubMed: 10191116]

Mole SE, Williams RE, Goebel HH. Correlations between genotype, ultrastructural morphology and clinical phenotype in the neuronal ceroid lipofuscinoses. Neurogenetics 2005;6:107–126. [PubMed: 15965709]

Mrak RE, Griffinbc WS. The role of activated astrocytes and of the neurotrophic cytokine S100B in the pathogenesis of Alzheimer's disease. Neurobiol Aging 2001;22:915–922. [PubMed: 11754999]

Pontikis CC, Cotman SL, MacDonald ME, Cooper JD. Thalamocortical neuron loss and localized astrocytosis in the Cln3Deltaex7/8 knock-in mouse model of Batten disease. Neurobiol Dis 2005;20:823–836. [PubMed: 16006136]

Rothermundt M, Peters M, Prehn JH, Arolt V. S100B in brain damage and neurodegeneration. Microsc Res Tech 2003;60:614–632. [PubMed: 12645009]

Santavuori P, Haltia M, Rapola J. Infantile type of so-called neuronal ceroid-lipofuscinosis. Dev Med Child Neurol 1974;16:644–653. [PubMed: 4371326]

Santavuori P, Haltia M, Rapola J, Raitta C. Infantile type of so-called neuronal ceroid-lipofuscinosis. 1. A clinical study of 15 patients. J Neurol Sci 1973;18:257–267. [PubMed: 4698309]

Sarna J, Miranda SR, Schuchman EH, Hawkes R. Patterned cerebellar Purkinje cell death in a transgenic mouse model of Niemann Pick type A/B disease. Eur J Neurosci 2001;13:1873–1880. [PubMed: 11403680]

Sarna JR, Hawkes R. Patterned Purkinje cell death in the cerebellum. Prog Neurobiol 2003;70:473–507. [PubMed: 14568361]

Sleat DE, Wiseman JA, El-Banna M, Kim KH, Mao Q, Price S, Macauley SL, Sidman RL, Shen MM, Zhao Q, Passini MA, Davidson BL, Stewart GR, Lobel P. A mouse model of classical late-infantile neuronal ceroid lipofuscinosis based on targeted disruption of the CLN2 gene results in a loss of tripeptidyl-peptidase I activity and progressive neurodegeneration. J Neurosci 2004;24:9117–9126. [PubMed: 15483130]

Slemmer JE, Haasdijk ED, Engel DC, Plesnila N, Weber JT. Aldolase C-positive cerebellar Purkinje cells are resistant to delayed death after cerebral trauma and AMPA-mediated excitotoxicity. Eur J Neurosci 2007;26:649–656. [PubMed: 17686042]

Switzer RC 3rd. Application of silver degeneration stains for neurotoxicity testing. Toxicol Pathol 2000;28:70–83. [PubMed: 10668992]

Taupin P. HuCNS-SC (StemCells). Curr Opin Mol Ther 2006;8:156–163. [PubMed: 16610769]

Vanhanen SL, Sainio K, Lappi M, Santavuori P. EEG and evoked potentials in infantile neuronal ceroid-lipofuscinosis. Dev Med Child Neurol 1997;39:456–463. [PubMed: 9285436]

Vesa J, Hellsten E, Verkruyse LA, Camp LA, Rapola J, Santavuori P, Hofmann SL, Peltonen L. Mutations in the palmitoyl protein thioesterase gene causing infantile neuronal ceroid lipofuscinosis. Nature 1995;376:584–587. [PubMed: 7637805]

Wainwright MS, Craft JM, Griffin WS, Marks A, Pineda J, Padgett KR, Van Eldik LJ. Increased susceptibility of S100B transgenic mice to perinatal hypoxia-ischemia. Ann Neurol 2004;56:61–67. [PubMed: 15236402]

Welsh JP, Yuen G, Placantonakis DG, Vu TQ, Haiss F, O'Hearn E, Molliver ME, Aicher SA. Why do Purkinje cells die so easily after global brain ischemia? Aldolase C, EAAT4, and the cerebellar contribution to posthypoxic myoclonus. Adv Neurol 2002;89:331–359. [PubMed: 11968459]

Worgall S, Sondhi D, Hackett NR, Kosofsky B, Kekatpure MV, Neyzi N, Dyke JP, Ballon D, Heier L, Greenwald BM, Christos P, Mazumdar M, Souweidane MM, Kaplitt MG, Crystal RG. Treatment of late infantile neuronal ceroid lipofuscinosis by CNS administration of a serotype 2 adeno-associated virus expressing CLN2 cDNA. Hum Gene Ther 2008;19:463–474. [PubMed: 18473686]

Zhang Z, Butler JD, Levin SW, Wisniewski KE, Brooks SS, Mukherjee AB. Lysosomal ceroid depletion by drugs: therapeutic implications for a hereditary neurodegenerative disease of childhood. Nat Med 2001;7:478–484. [PubMed: 11283676]

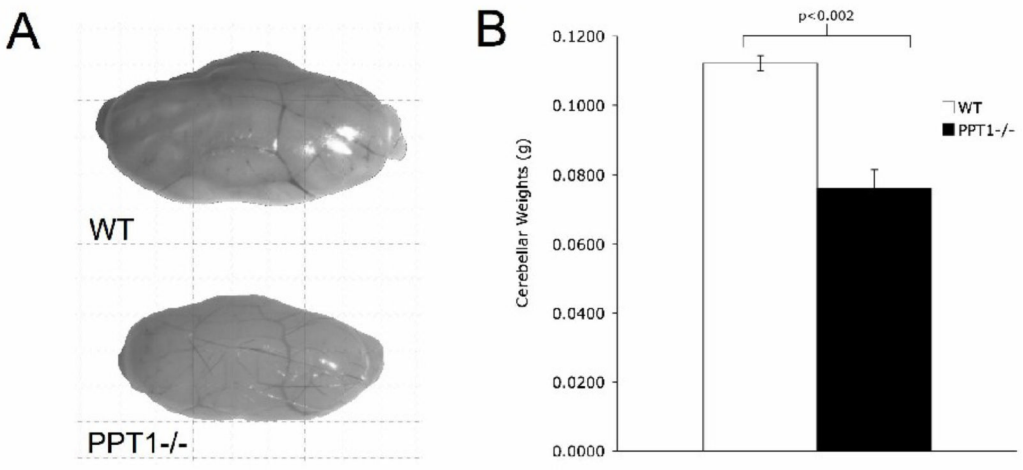

Figure 1.

An overall atrophy is observed in the PPT1−/− cerebellum at 7 mo. of age. (A) Representative images of PPT1−/− and wildtype cerebella. Notice the size differential between the mutant and wildtype control. (B) Quantification of the cerebellar weights in PPT1−/− (n=5) and wildtype mice (n=5) revealed a statistically significant decrease in cerebellar mass in PPT1−/− mice compared to wildtypes ($p<0.002$).

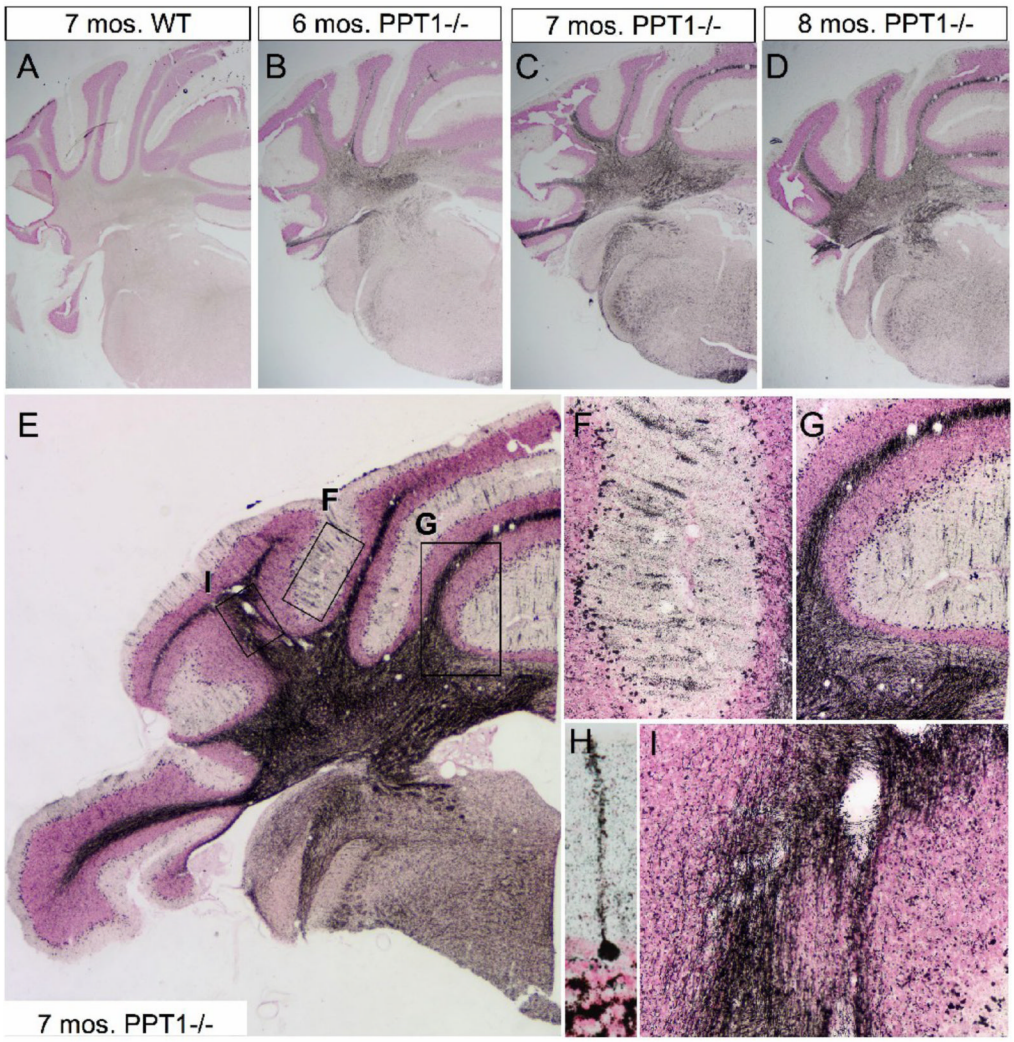

Figure 2.

DeOlmos cupric silver degeneration staining in PPT1−/− mice. (A–D) Representative coronal images of silver staining in the anterior cerebellum of WT (A), 6 mo. PPT1−/− (B), 7 mo. PPT1 −/− (C), and 8 mo. PPT1−/− mice (D). Notice the overall increase in silver staining as the mice age, most notably within the cerebellar white matter. (E) Higher magnification image of the 7 mo. PPT1−/− cerebellum. In addition to the cerebellar white matter, silver stained parasagittal bands, or blackened stripes, are visualized in the molecular layer in the cerebellar cortex. Locator boxes identify the areas magnified in subsequent panels. (F & G) High magnification of parasagittal banding found in an individual folia of PPT1−/− mice at 7 mo. The banding seen in the molecular layer is staining of the dendritic arbors of diseased Purkinje cells. Blackened debris litters the Purkinje cell layer, most likely due to dying Purkinje cells. (H) High magnification of a degenerating Purkinje cell, with a blackened soma and dendritic arbor. (I) High magnification image of the cerebellar white matter tracts contains degenerating efferent and afferent projections to the cerebellar cortex. Degenerating axons represent the sole output of the PPT1−/− cerebellum.

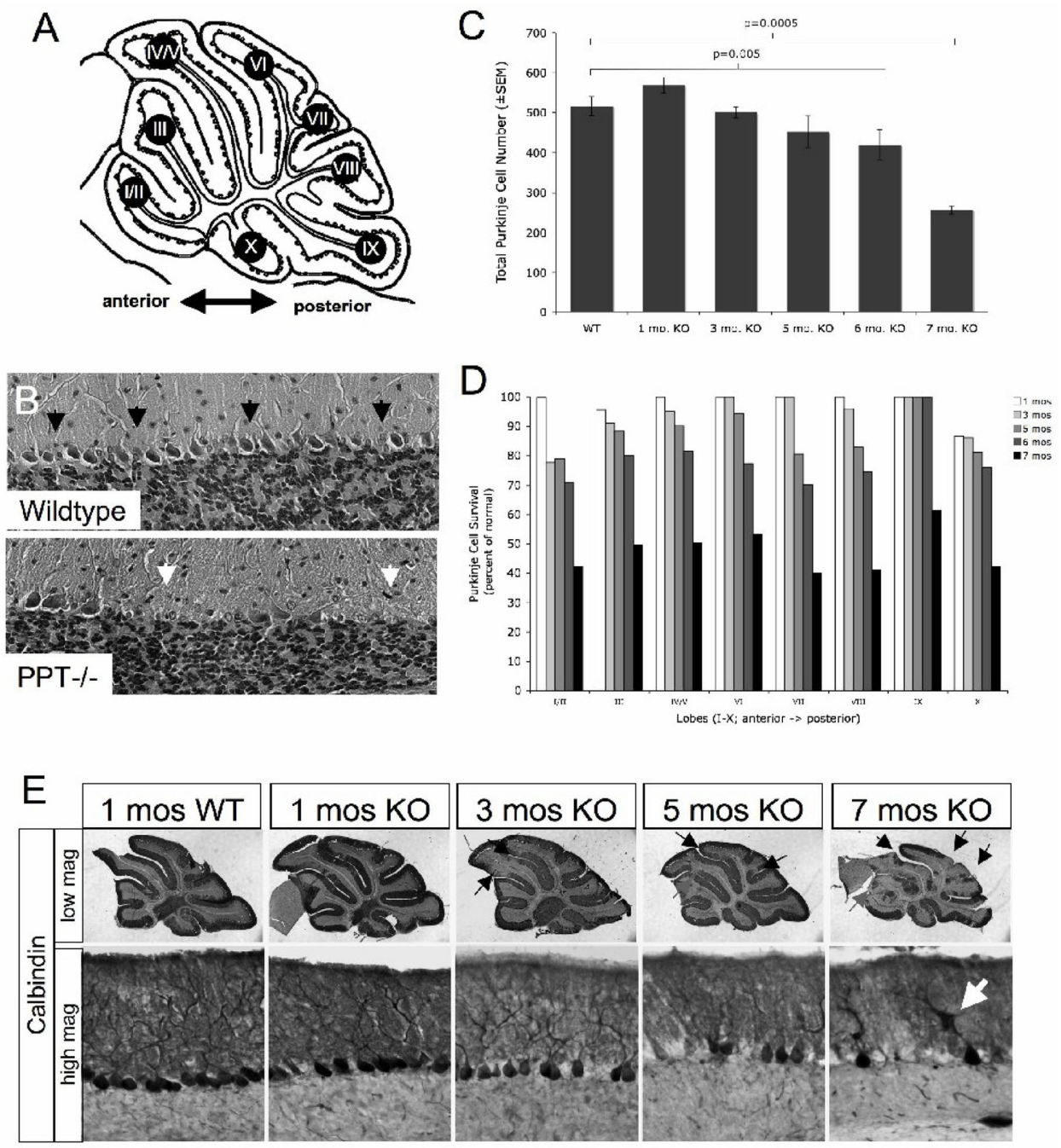

Figure 3.

Purkinje cell loss in the PPT1−/− cerebellum. (A) Schematic representation of lobes I-X of the cerebellar vermis. (B) H&E stained cerebella from PPT1−/− and wildtype mice. Black arrows indicate a contiguous Purkinje cell monolayer present in WT cerebellum. In the PPT1−/− cerebellum, white arrows indicate patches of missing Purkinje neurons. (C) Graphical representation of Purkinje cell survival (total cell number±SEM) in PPT1−/− cerebella at 1, 3, 5, 6, and 7 mo. of age. (D) Purkinje cell survival by lobe (as a percent of normal) in 1, 3, 5, 6, and 7 mo. PPT1−/− mice. (E) Calbindin staining in the PPT1−/− cerebellum. At low magnification, there were comparable levels of staining in a 1 mo. WT and PPT1−/− cerebellum. By 3 mo. of age, loss of calbindin staining appeared in patches throughout the

anterior cerebellum (arrows). By 7 mo. of age, nearly half of the cerebellum lacked calbindin immunoreactivity. At high magnification, the molecular and Purkinje cell layers of 1 mo. WT and PPT1−/− cerebella appeared normal with darkly stained Purkinje cell bodies and dendritic arbors. As the mice age, there was a decrease in the intensity of calbindin staining, a denudation of the Purkinje cell layer and pruning of the dendritic arbors. The white arrow identifies a swollen dendrite. Comparable levels of calbindin staining were observed in 1, 3, 5, 6, and 7 mo. wildtype mice.

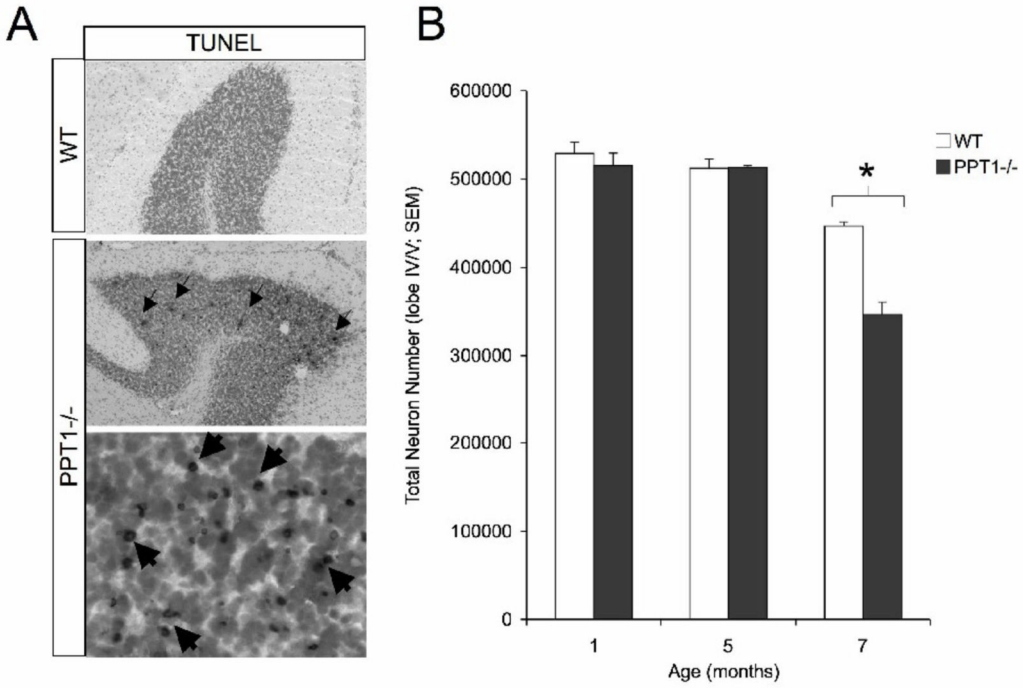

Figure 4.

Cell loss in the granular cell layer. (A) TUNEL-positive cells were found in the granular cell layer (GCL) of the 7 mo. PPT1−/− cerebellum. Nuclear fast red staining identified cells within the granular cell layer at low magnification. At high magnification, numerous darkly stained, TUNEL + profiles were observed throughout the GCL (dark staining; arrows). (B) Quantification of the granular cell number demonstrated a statistically significant ($p<0.05$; asterisk) cell loss at 7 mo. of age, with no changes in total cell number evident before this age. No TUNEL positive cells were observed in 1, 3, 5, 6, and 7 mo. wildtype mice.

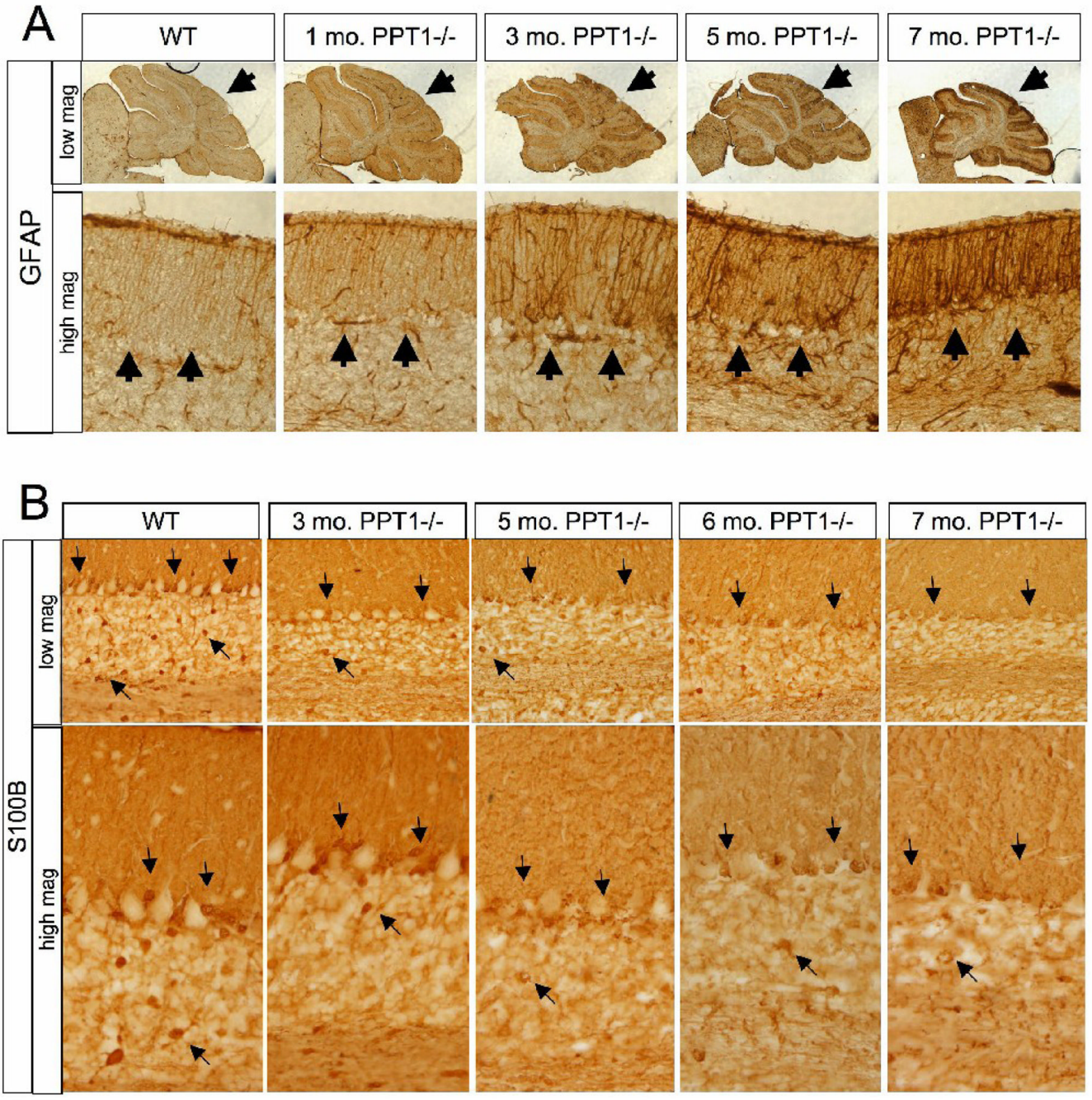

Figure 5.

Astrocyte changes in the PPT1−/− cerebellum. (A) GFAP staining was performed on 1, 3, 5, and 7 mo. PPT1−/− cerebella. Astrocyte activation was found in PPT1−/− mice as early as 1 mo. of age, with a diffuse increase in GFAP immunoreactivity. By 3 mo. of age, there was a hypertrophy of astrocytic processes and patches of GFAP upregulation through the PPT1−/− cerebellum (black arrows). This phenomenon continues as the mice age. Comparable levels of GFAP staining were observed in 1, 3, 5, 6, and 7 mo. wildtype mice. (B) Astrocyte dysfunction in the PPT−/− mouse. S100β staining was performed on 1, 3, 5, 6, and 7 mo. PPT1−/− cerebella. Compared to WT, there was an overall decrease in S100β by 5 mo. of age (black arrows). Most

notably, there was a progressive loss of immunoreactivity in the Bergmann glia and astrocytes of the granular cell layer.

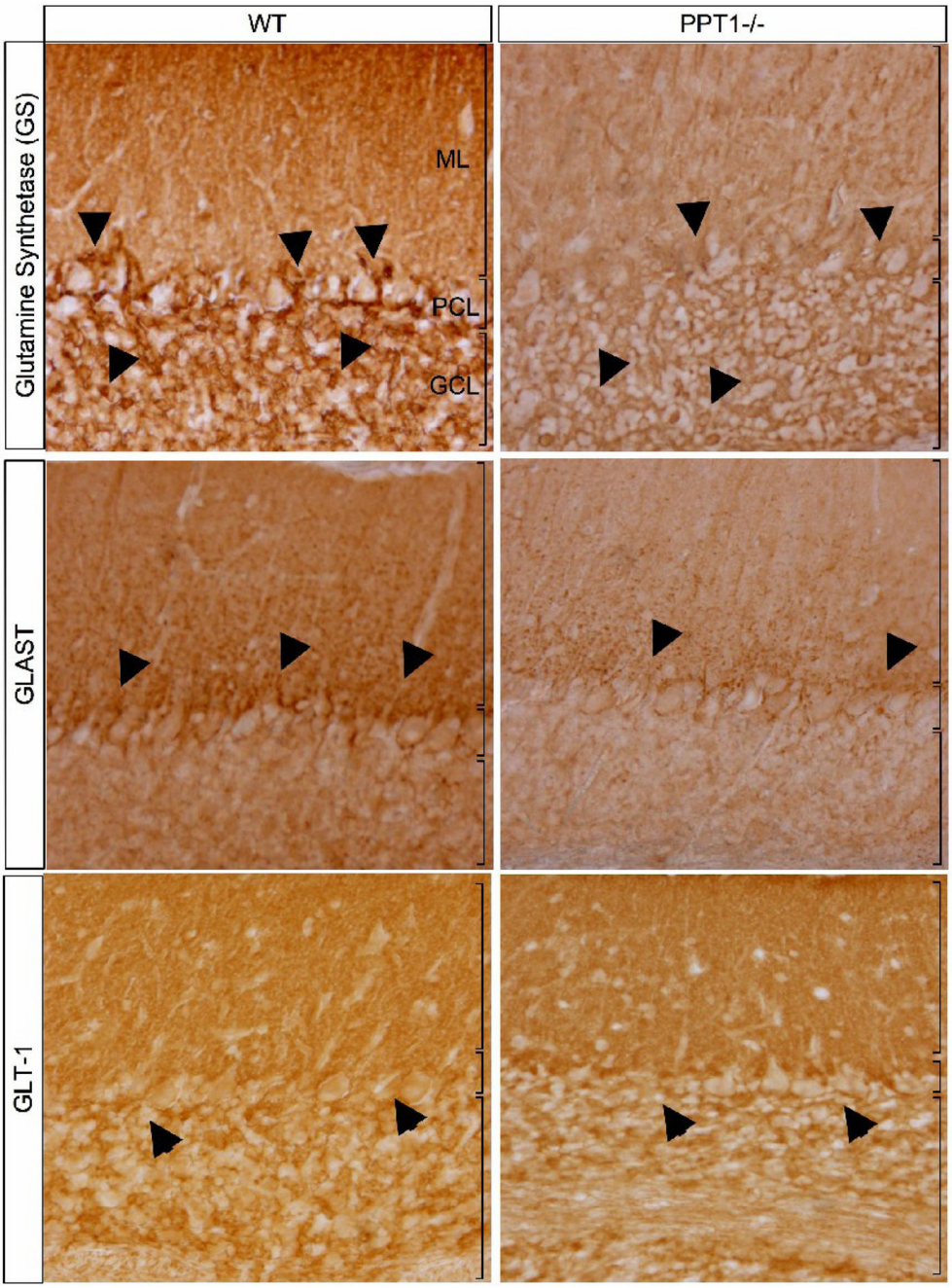

Figure 6.

Glutamine synthetase (GS), GLAST, and GLT-1 staining in 7 mos. PPT1−/− and WT mice. An apparent loss of GS staining was observed in the cerebellar cortex of 7 mos. PPT1−/− mice. Most notably, there was a loss of staining within the cell bodies of the Bergmann glia (black arrows). GLAST staining in PPT1−/− mice demonstrated a diffuse, overall reduction in immunoreactivity compared to WT. A decrease in GLAST expression in the Bergmann glia (arrows) and the molecular layer was also apparent. In contrast, GLT-1 staining was comparable levels in WT and PPT1−/− mice. A notable exception is the intensity of staining in the Purkinje cell layer, which was markedly reduced.

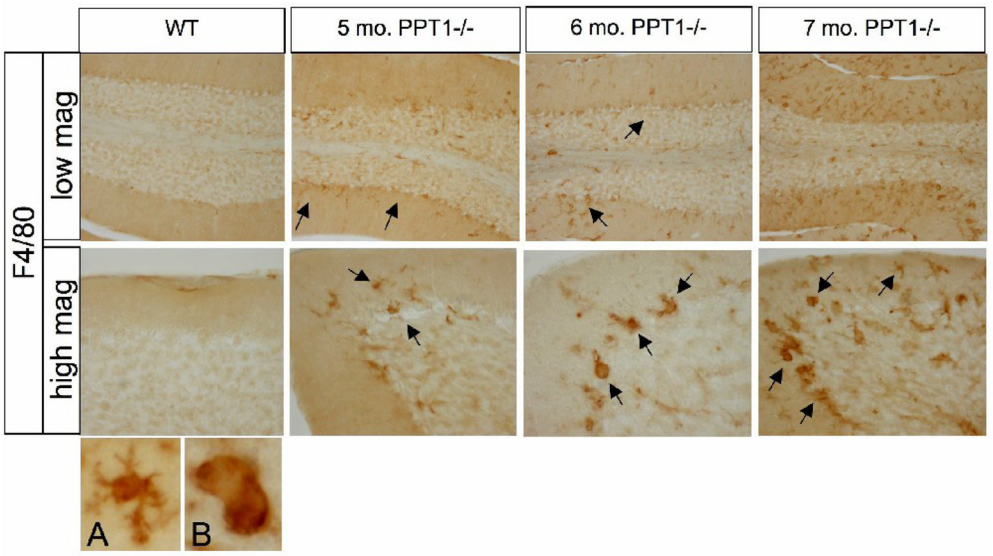

Figure 7.

F4/80 staining, a monocyte marker, in PPT1−/− and wildtype mice. PPT1−/− mice showed an increase in the number of monocytes starting at 5 mos. of age. As the mice age, there was an increase in monocytes at 6 and 7 mos. (black arrows). In addition, there was a change in the morphology of the F4/80 positive cells from small, ramified cells with a microglial morphology (A) to larger rounded brain macrophage-like cells (B). Comparable levels of F4/80 staining were observed in 1, 3, 5, 6, and 7 mo. wildtype mice.

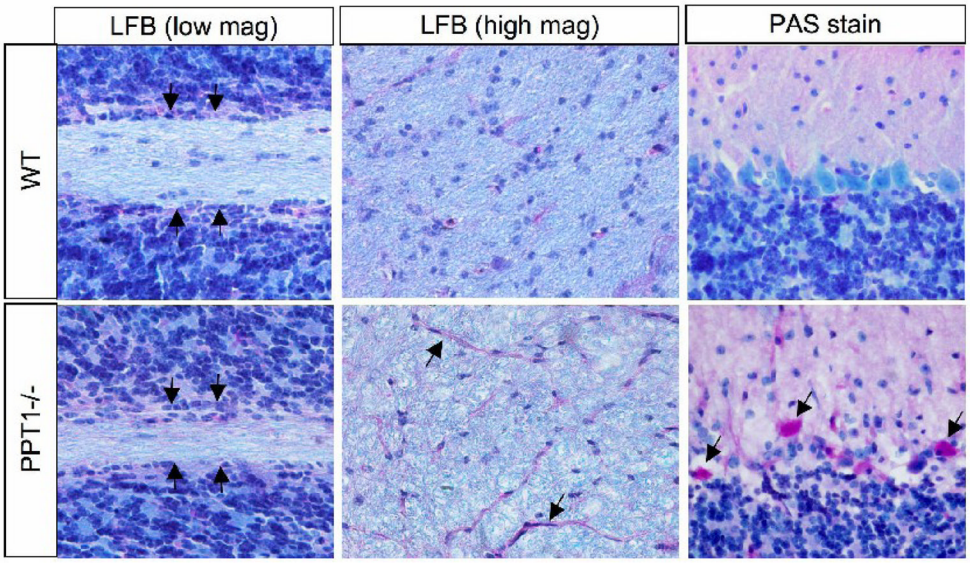

Figure 8.

Luxol Fast Blue (LFB) and Periodic acid-Schiff (PAS) staining in the PPT1−/− cerebellum. Staining for the myelin marker, luxol fast blue, was markedly decreased in PPT1−/− mice at 7 mo. At low magnification, there was a thinning of the cerebellar white matter tracts in the PPT1−/− mice compared to WT. At high magnification, the intensity of staining and organization of the white matter was disrupted in the PPT1−/− cerebellum. PAS staining (red) demonstrated glycogen inclusions in the molecular layer and Purkinje cell layers of PPT1−/− mice. In addition, the vasculature in the white matter tracts was PAS positive (arrows).

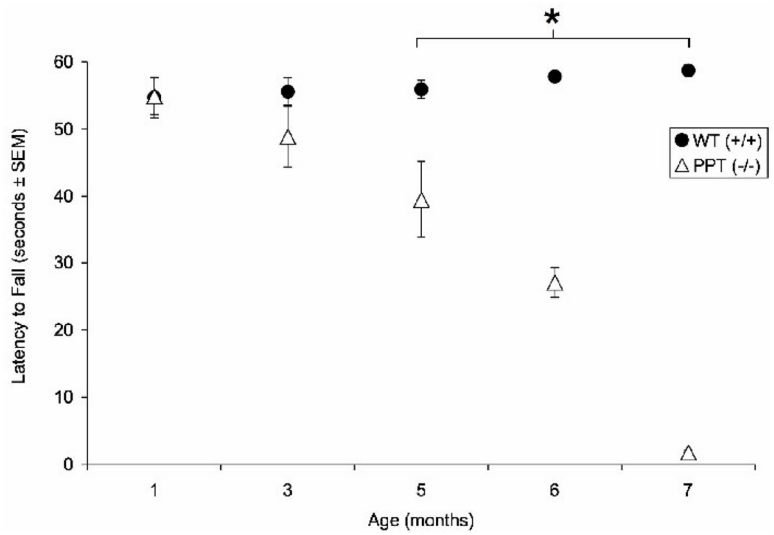

Figure 9.

Constant speed rotarod testing in the PPT1−/− mice. PPT1−/− mice display sigficant motor deficits ($p<.0.0005$) on the rotarod tests beginning at 5 mo. of age, and continuing through 6 ($p<.0.0005$) and 7 ($p\leq0.001$) months of age. The asterisk denotes statistical significance. WT mice performed at criterion for the entire task.